Weather and Climate Extremes 23 (2019) 100195

Contents lists available at ScienceDirect

Weather and Climate Extremes

journal homepage: www.elsevier.com/locate/wace

Evaluation of summer monsoon climate predictions over the Indochina Peninsula using regional spectral model

Thang V. Nguyen[a], Khiem V. Mai[a], Phuong N.B. Nguyen[a,*], Hann-Ming H. Juang[b], Duc V. Nguyen[a]

[a] Vietnam Institute of Meteorology, Hydrology and Climate Change, Hanoi, Vietnam
[b] National Centers for Environmental Prediction, NWS, NOAA, Washington, D.C, United States

ARTICLE INFO

Keywords:
Summer monsoon
Regional spectral model
Indochina peninsula
Onset
Climate prediction
Maximum temperature
Minimum temperature
Maximum 1-day rainfall

ABSTRACT

Monsoons are a major component of the global climate system affecting floods, droughts and other climate extremes. In this study, we investigated the performance of RSM (Regional Spectral Model) for predicting the summer monsoon over the Indochina Peninsula (ICP) region from 1982 to 2010. The NCEP - Climate Forecast System Reforecast (CFS-reforecast) was used to provide initial and boundary forcing for the RSM configured with an approximately 26 km grid over the ICP. The large-scale fields as well as surface temperature and rainfall of RSM have been evaluated for differing El Niño-Southern Oscillation (ENSO) years. The factors affecting changes in the rainfall patterns in ENSO years were determined using the empirical orthogonal function method. In addition, the ability of forecasting onset of summer monsoon was assessed based on the changes in outgoing longwave radiation, rainfall and average zonal wind at 850 hPa. The RSM is satisfactory in terms of forecasting large-scale features in different ENSO conditions. It produces well the interaction between Southwest and Southeast airflow, which are the main characteristics of summer monsoon throughout the study area. The RSM reforecasts are compared to CRU (Climatic Research Unit) data for the distribution of temperature and precipitation; however, their changes due to ENSO condition is inconsistent with CRU data. The extremes maximum and minimum temperatures have reverse signals with ENSO conditions. The extremes maximum 1-day rainfall have a significant change over the gulf of Tonkin and western ICP area due to ENSO condition. RSM results have indicated the effects of terrain and the reverse effects of ENSO condition over ICP area. The onset of summer monsoon is later in summer of El Niño year when compared with the other conditions.

1. Introduction

Over the Indochina Peninsula (ICP) region, climate is characterized by the interaction among various monsoon systems, such as East Asian summer monsoon (EASM), Indian summer monsoon (ISM), Northwest pacific summer monsoon (WNPSM) and Qinghai-Tibet Plateau monsoon (Webster and Yang, 1992; Ju and Slingo, 1995; Wang, 2002). In summer, the low-wind directions are south-westerlies over western and southern ICP, caused by ISM and WNPSM; while the low-wind directions are south-easterlies over northern and eastern ICP, caused by EASM. Therefore, climate patterns in the western and southern ICP are affected by a large scale shift of convection and heat source from ISM; Whereas, climate patterns in the northern and eastern are affected by land-sea thermal contrast, which induced the edge of the western Pacific subtropical High. The southwestern low-wind derives from the North Indian Ocean and bring airflows with very high humidity to ICP area (Nguyen, 2017). The southern low-wind derived from margin of Western-north Pacific Sub-tropical High converges with the southwestern low-wind resulting in the instability of the air mass over the study area. The convergence of two near-horizontal airflows in the direction of horizontal motion is the characteristic of the summer monsoon in this region.

Furthermore, climate in this region is closely associated with El Niño-Southern Oscillation (ENSO), which affects strongly to monsoon activities. During the El Niño years, the Pacific Warm Pool is expanded eastward; deep convection system over the western tropical Pacific is replaced by relatively high-pressure system. This change results in altering the monsoon systems (i.e. ISM with El Niño is weak due to the weakening of western wind derived from trade wind). In turn, changes in the ocean and monsoon circulations can forewarn rainfall patterns. Consequently, the summer rainfall season over the ICP in an El Niño year tends to be lesser than other years. In contrast, La Niña impacts

* Corresponding author.
E-mail address: nn.bichphuong@gmail.com (P.N.B.,. Nguyen).

https://doi.org/10.1016/j.wace.2019.100195
Received 21 July 2018; Received in revised form 19 December 2018; Accepted 13 January 2019
Available online 19 January 2019

show opposite trends compared to those of El Niño. For example, Walker circulation appears to be stronger with La Niña. As a result, the deep convection system over the western tropical Pacific is enhanced, which leads to above-average rainfall over Maritime Continent and the ICP (e.g. Ju and Slingo, 1995; Zhang et al., 2002; Zhou and Chan, 2007). In addition, the orographic system over this area can affect directly rainfall regimes. This is interpreted by the variations in intensity of monsoon precipitation along coastal regions with orographic barriers in some studies (e.g. Matsumoto 1997; Wang, 2002; Nguyen-Le et al. 2014).

Global climate models are commonly used with the resolution of about 100 km. However, such resolution is relatively coarse and insufficient to describe the climate characteristics of numerous regions in the world, especially in terms of areas with complex terrain. For this reason, the use of regional climate models with a finer horizontal resolution seems to be better to simulate climate variations for these regional areas. In this study, Regional Spectral Model (RSM) was used as a high-resolution regional climate model to simulate and predict the climate in the ICP region.

The objective of this study was to investigate the performance of RSM in predicting summer monsoon throughout the ICP region. To investigate the performance of RSM, we have used the NCEP - Climate Forecast System Reforecast (CFS-reforecast) to providing large-scale forcing for the RSM configuration with a horizontal resolution of about 26 km over ICP. This study compared average climate variables in summer of El Niño years, non-ENSO years and La Niña years at 850, 700, 500 hPa and surface to detect the signals of El Niño and La Niña. In addition, the rainfall from RSM reforecast was compared with CRU data, which have a horizontal resolution of 0.5°.

2. RSM model, data and methodology

2.1. RSM model

It is noted that RSM is a limited area atmospheric numerical model system, which was fully developed inside the National Centers for Environmental Prediction (NCEP), based on the structure of the NCEP Global Spectral Model (Juang and Kanamitsu, 1994). This model is primarily used for daily weather forecasts, and climate simulations or predictions. Currently, RSM consists of two separate dynamic options, including hydrostatic or non-hydrostatic dynamics. The hydrostatic version is known as a RSM, whereas the non-hydrostatic version is known as a meso-scale spectral model (MSM) as reported by Juang (2000). In this study, the non-hydrostatic version of RSM (MSM) was used for further simulations. The model equations consist of three momentum equations, a thermodynamic equation, a mass conservation equation and a moisture equation. The RSM applies sine and cosine series to the deviation of the full forecast field from the global base field (perturbations), which can be very accurate and efficient spectral calculations. The detail description can be found in Juang and Kanamitsu (1994) and Juang (2000). In this version, numerical methods consist of the perturbation method, spectral computation, fourth-order horizontal diffusion, implicit lateral boundary relaxation, a time filter, and semi-implicit adjustment. Compared to MSM, some modification as instead of using equal weighted coefficients for semi-implicit integration, a forward-time-weighted semi-implicit scheme is used. The physics schemes of RSM used in this study are long-wave radiation scheme (Mlawer et al., 1997), short-wave radiation scheme (Chou and Suarez, 1999), deep convection (Grell, 1993), planetary boundary layer processes (Troen and Mahrt, 1986) and the Noah land surface model (Ek et al., 2003).

Juang and Hong (2001) had evaluated the performance of RSM model through the sensitivities of different model domain sizes and horizontal resolutions. This study has demonstrated that RSM model in regional domain has successful long-range integration because the lateral boundary errors are relatively small and the large-scale waves are preserved through the domain and spectral nesting.

In addition, the RSM with regional domain could generate higher resolution feature than its base field (outer coarse –resolution global model T126). Han and Roads (2004) used RSM model to evaluate a seasonal climate forecast over northern South America, encompassing the rainy season over Brazil' Nordeste. This study summarized that the regional model at 80-km resolution improves upon the AGCM rainfall forecast, reducing both seasonal bias and root-mean-square error; However, the RSM with 20-km resolution forecasts presented larger errors, with spatial patterns that resemble those of local topography. Zhang et al. (2005) evaluated the Coupled NCEP RSM and an advance land surface model (LSM) over the Hawaiian Islands. This study has shown that overestimation of the surface wind speed and daytime cold biases experienced by the RSM are largely corrected by coupling the RSM with the LSM. The study has indicated that the high-resolution RSM–LSM has better capability in simulating localized rainfall distributions and airflows associated with the heavy rainfall event.

In Vietnam, the RSM model system has been used by the Viet Nam Institute of Meteorology, Hydrology and Climate Change (IMHEN) for researching and operating climate forecast since 2011, when the NCEP team visited and worked at the IMHEN for the application of the NCEP's RSM/CFS seasonal climate forecasting system.

2.2. Data

2.2.1. Climate forecast system reanalysis (CFSR)

Climate Forecast System Reanalysis (CFSR) is the global reanalysis with high horizontal resolution at the National Centers for Environmental Prediction (NCEP), completed over 30 years from 1982 to 2010. The CFSR was designed and executed as a global, high resolution, coupled atmosphere-ocean-land surface-sea ice system to provide the best estimation of the state of these coupled domains. The CFSR global atmosphere, oceanic and land surface output products are available at 0.5 × 0.5-degree latitude and longitude resolution with 64 levels extending from the surface to 0.26 hPa. The global ocean is 0.25° at the equator, extending to a global 0.5° beyond the tropics, with 40 levels to a depth of 4737 m. The global land surface model has 4 soil levels and the global sea ice model has 3 levels. The CFSR atmospheric model also contains observed variations in carbon dioxide (CO_2), together with changes in aerosols and other trace gases and solar variations (Saha et al., 2010).

2.2.2. Climate forecast system (CFS) reforecast

NCEP Climate Forecast System version 2 (CFSv2) is the fully coupled ocean–land–atmosphere dynamical seasonal prediction system, which made operational at NCEP in March 2011. In this study, we have used CFS reforecasts to generate initial conditions for the model. The data are the 6-month re-forecasted data with starting months at April, May, and June for 29 years from 1982 to 2010. The identification of ENSO and non-ENSO was based on the monthly mean sea surface temperature anomalies greater than (less than) 0.5 °C for the Oceanic Nino Index (ONI) [3 month running mean of ERSST.v5 SST anomalies in the Nino 3.4 region (5ºN-5ºS, 120º-170ºW)] (Table 1). Therefore, the summers with El Niño include years of 1982, 1987, 1991, 1997, 2002, 2004 and 2009; the summers with non-ENSO include years of 1983, 1984, 1989, 1990, 1992, 1993, 1994, 1995, 1996, 2001, 2003, 2005, 2006 and 2008; and the summer with La Niña comprise years of 1985, 1988, 1998, 1999, 2000, 2007, 2010. These datasets include surface and radiative fluxes (FLXF) and 3-D pressure level variables (PGBF) files, output time step is 6-h: 00, 06, 12, 18 UTC for 6 months. The data can be downloaded from the NOAA website (Saha et al., 2014).

2.2.3. Observation data

We have used high resolution gridded datasets, CRU (Climatic Research Unit) 0.5° x 0.5°, for surface air temperature and precipitation.

Table 1
Oceanic Niño Index (ONI) in three summer months (JJA) from 1982 to 2010 (NOAA).

Year	**1982**	**1983**	**1984**	**1985**	**1986**	**1987**	**1988**	**1989**	**1990**
ONI (JJA)	0.8	0.3	−0.3	−0.5	0.2	1.5	−1.3	−0.3	0.3
ENSO condition	El Niño	Non-ENSO	Non-ENSO	La Niña	Non-ENSO	El Niño	La Niña	Non-ENSO	Non-ENSO
Year	**1991**	**1992**	**1993**	**1994**	**1995**	**1996**	**1997**	**1998**	**1999**
ONI (JJA)	0.7	0.4	0.3	0.4	−0.2	−0.3	1.6	−0.8	−1.1
ENSO condition	El Niño	Non-ENSO	Non-ENSO	Non-ENSO	Non-ENSO	Non-ENSO	El Niño	La Niña	La Niña
Year	**2000**	**2001**	**2002**	**2003**	**2004**	**2005**	**2006**	**2007**	**2008**
ONI (JJA)	−0.6	−0.1	0.8	0.1	0.5	−0.1	0.1	−0.5	−0.4
ENSO condition	La Niña	Non-ENSO	El Niño	Non-ENSO	El Niño	Non-ENSO	Non-ENSO	La Niña	Non-ENSO
Year	**2009**	**2010**							
ONI (JJA)	0.5	−1.0							
ENSO condition	El Niño	La Niña							

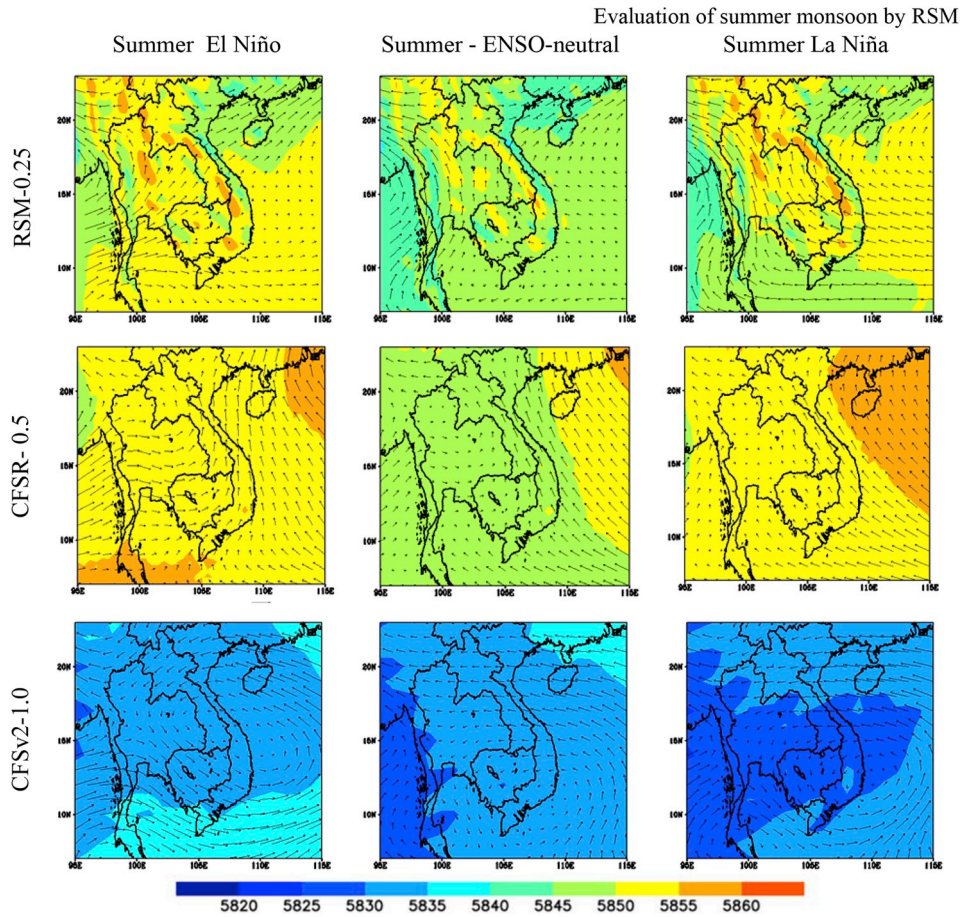

Fig. 1. Averaged geopotential height (m) and wind (m/s) at 500 hPa in summers (JJA) of El Niño/La Niña and ENSO-neutral condition Based on the result of RSM with horizontal resolution of 0.25° (RSM-0.25); CFSR with horizontal resolution of 0.5° (CFSR-0.5); CFSv2 with horizontal resolution of 0.25° (CFSv2-1.0).

These datasets have been developed and updated by Climatic Research Unit institution, which widely used in climate research (Harris et al., 2014). In this study, the datasets are 3-month (from June to August) of 29 years from 1982 to 2010.

2.3. Methodology

In this study, we have re-forecasted the summers in El Niño, La Niña and non-ENSO over ICP from 1982 to 2010 using a regional climate model, RSM. The identification of ENSO and non-ENSO was identified in section 2b. In Vietnam, the RSM model system has been used by the Viet Nam Institute of Meteorology, Hydrology and Climate Change (IMHEN) for researching and operating climate forecast since 2011, when the NCEP team visited and worked at the IMHEN for the application of the NCEP's RSM/CFS seasonal climate forecasting system. In this study, we have used RSM model to evaluate the local climate in summer with ENSO conditions. The RSM starts to run from May of each year and ends in September to have 3-month lead forecast for June to August (JJA) with one month for RSM spin-up time. In addition, we have re-forecasted 6-month with initializing in March and April for each year to detect the onset of summer monsoon over ICP.

To evaluate the RSM forecasts in ENSO and non-ENSO, we assess climate variabilities at 500,700, 850 hPa and surface by averaged climate variables in ENSO and non-ENSO years from 1982 to 2010. The re-forecasted surface temperature and rainfall were com-pared with CRU data. Besides, we have conducted the eigenvector patterns of two leading EOF modes of daily rainfall (EOF1 and EOF2) over ICP in summers of El Niño/La Niña and ENSO-neutral condition to detect factors that impact on rainfall regime over this area. In addition, we have assessed latitude time outgoing long wave radiation (latitude time

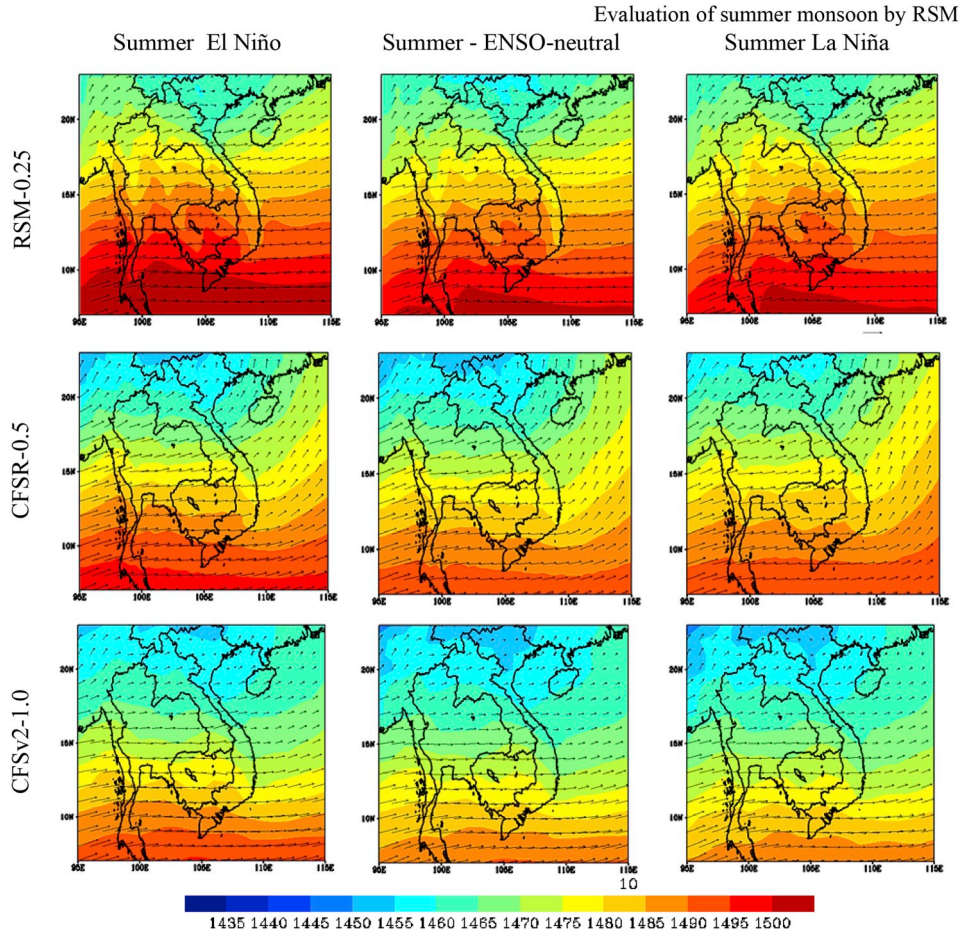

Fig. 2. Averaged geopotential height (m) and wind (m/s) at 850 hPa in summers (JJA) of El Niño/La Niña and ENSO-neutral conditions.

OLR) and average zonal wind at 850 hPa to identify the onset and withdraw of summer monsoon over ICP.

The RSM has used a domain with a horizontal resolution of 26 km cover Indochina Peninsula (ICP), as shown in Fig. 1. The number of grid points in Cartesian coordinates is 144 (west-east) and 144 (north-south). The domain size is 95E - 120E and EQ - 25N.

3. Result and discussions

In summer, climate system over ICP region is affected by the South Asian (or Iranian) low and Northwest pacific high; the South Asian low appears in April and is fully developed from June to August. The onset of monsoon in India and mainland Southeast Asia is related to changes in the circulation patterns that occur by June. The wind direction of east-west downturn depends on the weak-ending of each system. El Niño and La Niña phenomena occur in the equatorial Pacific region, affecting weather and climate in the ICP region. In this study, we assess the possibility of predicting monsoon, as well as capture the effects of El Niño and La Niña phenomenon of RSM model for the ICP region.

3.1. Large-scale features

The geopotential height (Hgt) approximates the actual height of the pressure level above mean seabed level. Hence, Hgt in a location will represent the height of the pressure level at that location. Because the cold air density is denser than the density of warm air, it makes the height of pressure level in cold air lower than in warm air.

Fig. 1 shows averaged Hgt and wind in summer El Niño, La Niña and non-ENSO of RSM (above), CFSR with horizontal resolution of 0.5° latlong (middle) and CFS-reforecast with horizontal resolution of 1° latlong (bottom) at 500 hPa over ICP. The figure indicates that winds and Hgt in the western ICP are influenced by a low pressure over the Bay of Bengal, while winds in the eastern ICP are influenced by the western pacific subtropical High. When comparing with CFSR, RSM produces proximity of winds and Hgt in the western ICP; However, there is a large distinction of wind in both direction and intensity over the eastern area. The winds and Hgt of RSM are incomparable with the ones of CFS-reforecast (initial condition).

When comparing the Hgt with ENSO conditions, Hgts with El Niño condition and La Niña are higher than the one with neutral condition of around 5 m. This demonstrates that El Niño and La Niña phenomenon leads to increase in temperature over the region. When compared with Hgt in CFSR and CFS-reforecast, Hgts of these areas increase about 10–15 m, whereas other areas increase in Hgts about 5–10 m. For wind speed and direction, RSM results seem compatible with those from CFSR. The wind speed and direction are slower and inappropriate with those of CFSR.

Fig. 2 depicts the averaged Hgt and wind at 850 hPa of RSM, CFSR 0.5° latitude-longitude and CFS-reforecast 1.0 latitude-longitude with El Niño, La Niña and non-ENSO. RSM reforecasts produce Hgt well when compared with those of CFSR in pattern from north to south; however, the values are higher by about 10 m. While, Hgt of CFS-reforecast is lower than Hgt of CFSR. The dynamical downscaling of CFS-reforecast by RSM leads to increase in Hgt values. The wind speed and direction in RSM seem to be the same as those of CFS-reforecast. CFSR shows higher wind speed than others. The wind direction in land of RSM is comparable with those of CFSR, which is the southwest monsoon thriving on the area; however, the wind direction over sea in CFSR is southwesterly, while the one in RSM has westward. With El Niño condition, Hgts are higher than other conditions about 5 m from the south to the north for all available data, RSM, CFSR and CFS-reforecast.

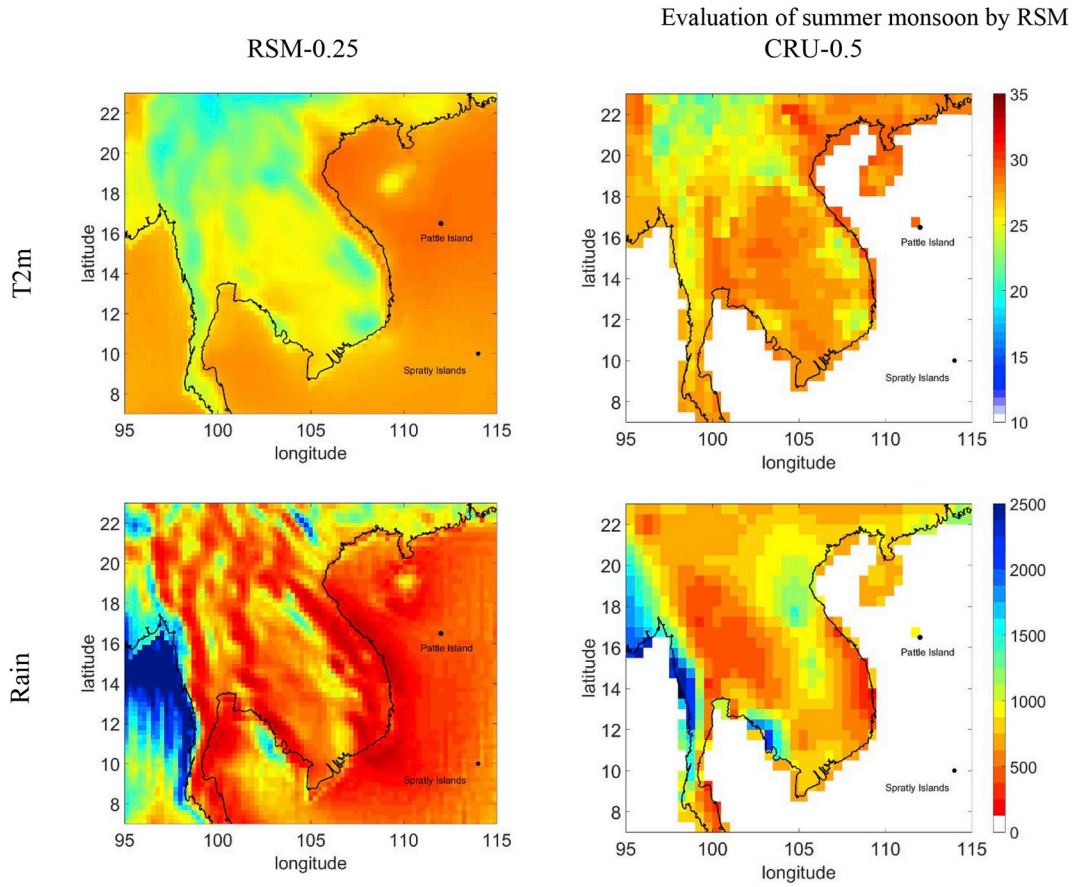

Fig. 3. Averaged surface air temperature (°C) and total rainfall (mm) of summers based on RSM-0.25 (left) and CRU with the horizontal resolution of 0.5° (CRU-0.5, right).

3.2. Surface air temperature

3.2.1. Averaged temperature

During the summer, ICP climate at the surface is influenced by the equatorial and tropical air masses, resulting from the high pressure of the southern hemisphere and tropical sea-air originating from the southwestern margin of western Pacific subtropical High. Surface air temperature is also influenced by terrain. The northwestern ICP and the East coast of Vietnam have hilly terrain, leading to lower temperatures in the area than others.

Fig. 3 shows the surface air temperature (above) and total summer rainfall (bottom) of the three summer months (JJA) from 1982 to 2010 for the ICP of the RSM data (left) and of the CRU (right). The results of the three-month summer rainfall forecast for the RSM model were compared with CRU 0.5° data to assess the predictability of the RSM model for these two variables.

For temperature, the result from RSM model is quite consistent with observation for spatial distribution; However, in terms of value, the temperature is predicted higher than that CRU data from 1-2 °C.

For rainfall, the RSM model shows that the spatial distribution is quite suitable with CRU data in the western and southern regions. However, forecasted rainfall for the North of RSM is not consistent in both quantity and distribution.

At the surface, RSM temperature is strongly influenced by the ENSO conditions and terrain in RSM (Fig. 4 above). The temperatures are reversal patterns with ENSO and terrain conditions. For example, with El Niño, surface air temperatures over Thailand, Cambodia and Laos decrease by 0.2–0.3 °C; and increase by 0.2–0.3 °C along Vietnamese coastline. While, with La Niña, the temperatures increase by 0.2–0.3 °C in Thailand, Cambodia and Laos; and decrease by 0.2–0.3 °C along Vietnamese coastline. However, the distribution of surface air temperatures in RSM is inconsistent with the ones of CRU. With El Niño, the CRU temperatures slightly changes in the range of −0.1 to 0.1 °C over Southern China and Vietnam. There is an increase of about 0.3 °C over Thailand. With La Niña, the temperatures increase by about 0.3 °C at over Laos, the North of Thailand and Vietnam, while decreasing of about 0.3 °C over the other areas. Nguyen D. N (2017) evaluated air surface temperatures with ENSO condition over Vietnam. This study has demonstrated the converse effects of ENSO conditions over central and southern Vietnam coastline. The result from RSM is in good agreement with Nguyen D. N (2017).

3.2.2. Extreme temperature

Figs. 5 and 6 shows the differences in averaged maximum and minimum surface air temperatures (Tx, Tn) between ENSO and non-ENSO. The extremes Tx over the region tend to have reversed signals. Over eastern Cambodia, southern Laos and southern Myanmar near Andaman sea, Tx decreases of 1-2 °C with El Niño; whereas, Tx tends to increase of 1-2 °C with La Niña. The reversed signals are also found over Vietnamese coastline and southwestern Thailand, in which Tx increases with El Niño and decreases with La Niña. The extremes Tn are also found over the ICP area, especially over Vietnamese coastline and Hainan island. Tn tends to increase with El Niño and decrease with La Niña about 0.5 - 1 °C.

3.3. Precipitation

3.3.1. Total rainfall

Fig. 7 presents the differences of total rainfall between ENSO and non-ENSO, in which the result of RSM is above, of CRU is middle and of

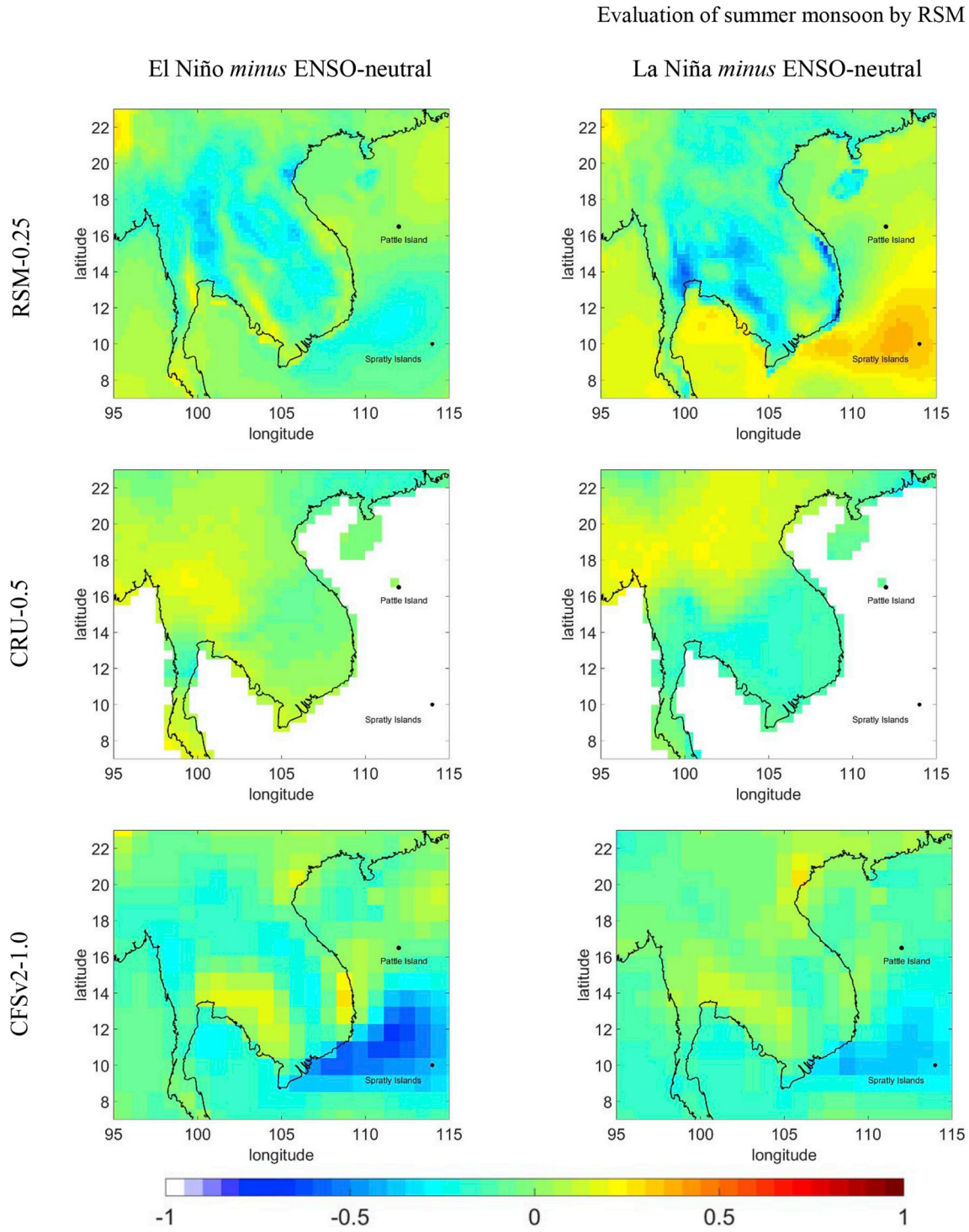

Fig. 4. Differences of average surface air temperature (°C) during summer (JJA) for different ENSO conditions of RSM-025 (above), of CRU-0.5 (middle) and CFSv2-1.0 (below).

GCM-CFS-1.0 is below. RSM reforecast provides an increase in rainfall over Andaman sea and some areas of Southern Laos with El Niño. With La Niña, the signals are opposite in the rainfall pattern. With CRU data, the distribution of rainfall is different with the one derived from RSM. The rainfall decreases about 200–300 mm over Thailand, Laos, Cambodia and Vietnam.

Figs. 8 and 9 provide the eigenvector patterns of two leading Empirical orthogonal function- EOF modes (EOF1, EOF2) of daily rainfall over ICP in summers of El Niño/La Niña and non-ENSO based on RSM and CFS reforecast. With El Niño and non-ENSO, disturbance waves appear to concentrate more and stronger than the one with La Niña. Particularly, in the case of El Niño, EOF1 pattern shows that the disturbance waves are mainly concentrated over the Andaman Sea and Myanmar. In the La Niña years, EOF1 pattern shows that the disturbance waves appear to be predominant over the southwest of ICP. EOF2 pattern shows the dense disturbance waves from the northeastern ICP and southwest over Andaman Sea.

It also can be seen in detail that, in Summer El Niño, the first EOF mode (EOF1) and the second EOF mode (EOF2) contribute 75% and 24.9% to the total variance, respectively. Similarly, in summer ENSO-

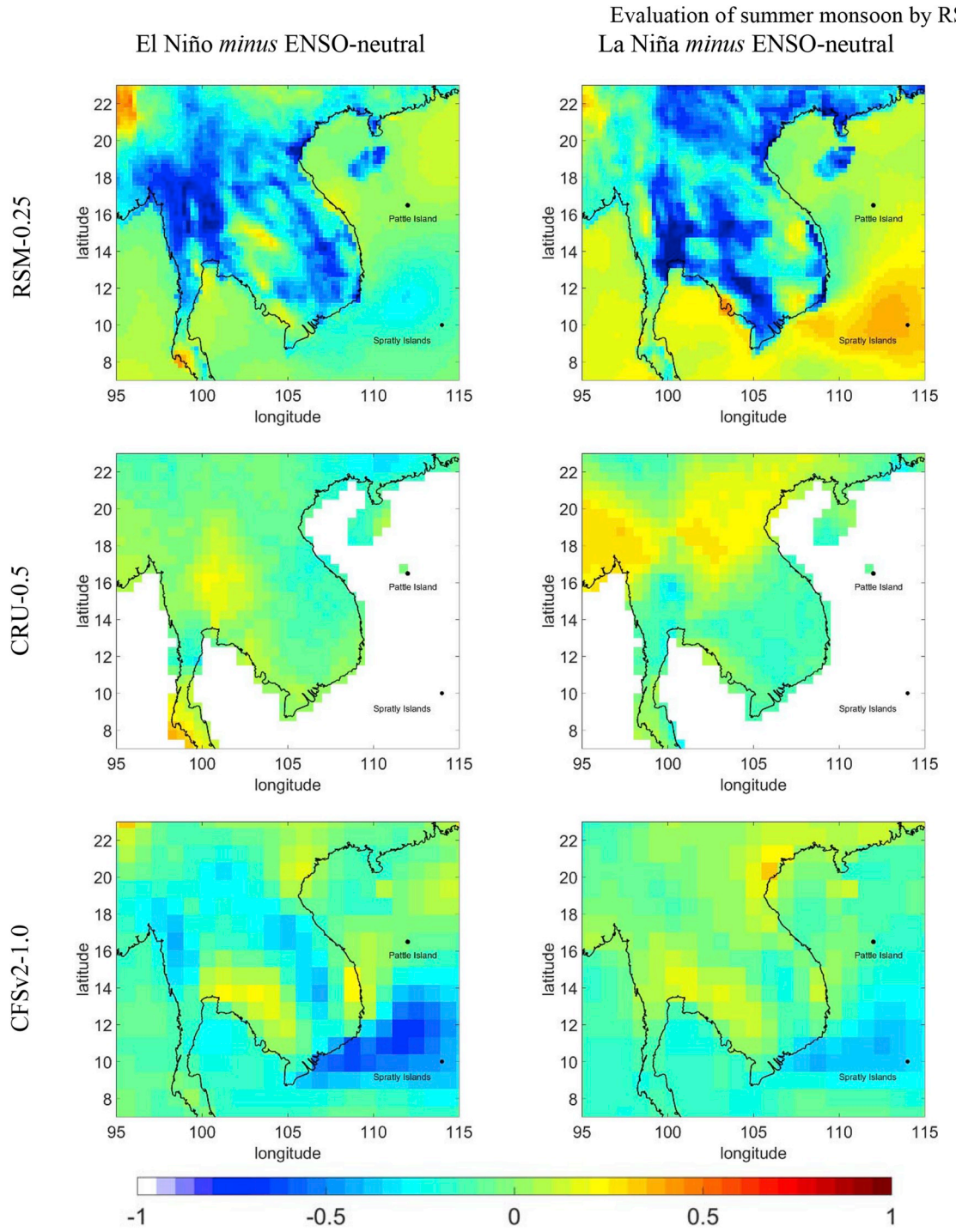

Fig. 5. Differences of average surface maximum air temperature (°C) during summer (JJA) for different ENSO conditions of RSM-025 (above), of CRU-0.5 (middle) and CFSv2-1.0 (below).

neutral cases, the EOF1 and EOF2 contribute 51.5% and 48.4% information to the total variance, respectively. In summer La Niña cases the EOF1 and EOF2 contribute 61.9% and 38% information, respectively. There are about 99.9% information in two modes for three different conditions. EOF1 represents the change of wind from the south to the north due to the activities of South Asian Low, and EOF2 represents the oscillatory waves in tropical monsoon winds cross the equator from the south and disturbances in the easterly wind field at the western margin of sub-tropical high pressure in Western Pacific.

From the analysis, in the case of El Niño, although the southwest winds dominate this zone in the summer, the summer rainfall is not only affected by the disturbances in the southwest winds. But also affected by the disturbances from the south, due to the Madden-Julian (MJO) oscillation with a 30–60-day cycle, which exists over the Eastern of Indian Ocean and the Western Pacific Equator affecting the Walker Circulation on the Pacific. In the case of La Niña, the summer rainfall is not only dominated by the disturbance waves from northeast due to the effects of high-pressure circulation over Pacific, but also affected by a great impact over the west and southwest due to the operation of the Southwest monsoon.

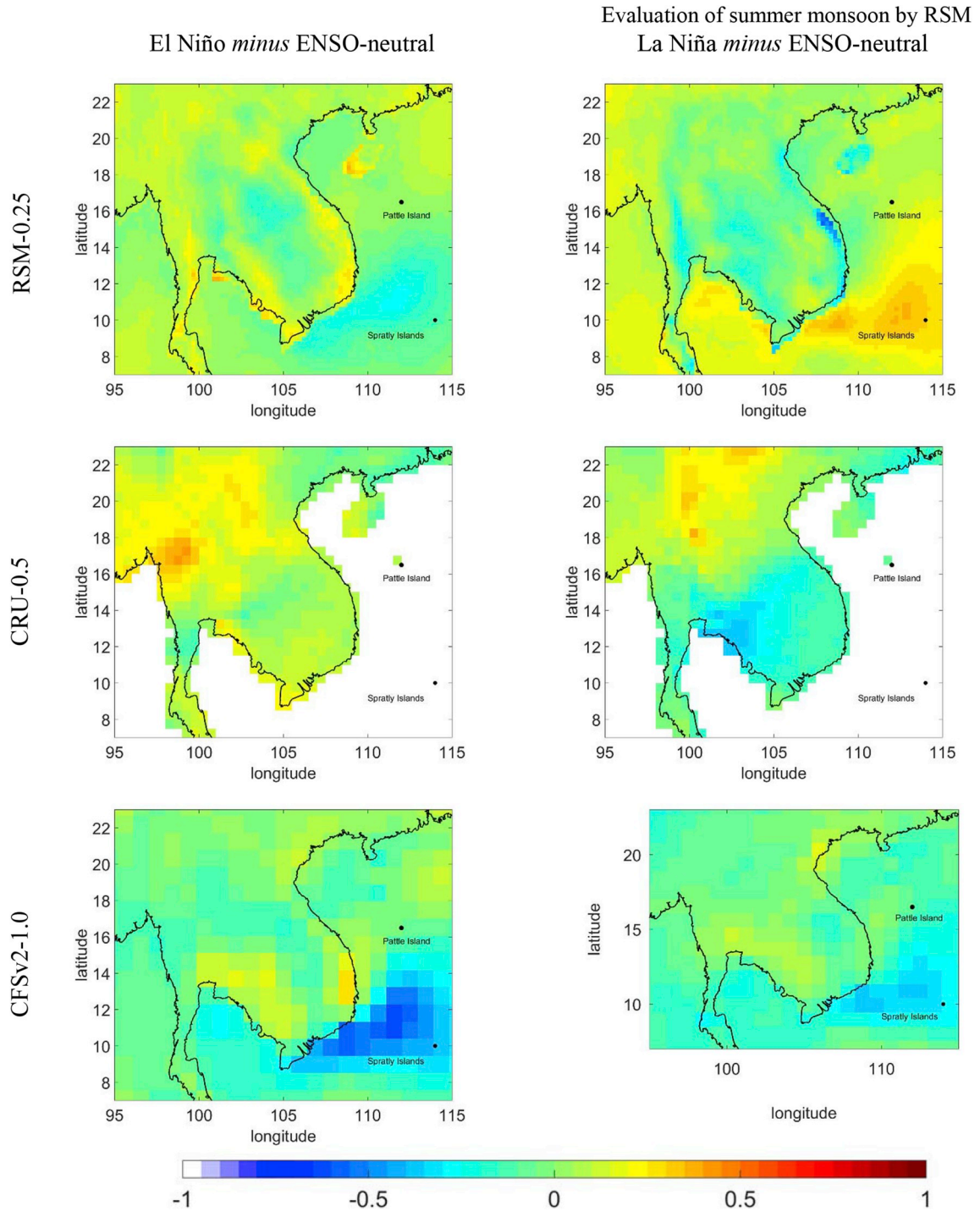

Fig. 6. Differences of average surface minimum air temperature (°C) during summer (JJA) for different ENSO conditions of RSM-025 (above), of CRU-0.5 (middle) and CFSv2-1.0 (below).

3.3.2. Maximum 1-DAY rainfall (RX1DAY)

Fig. 10 shows the differences in averaged maximum 1-day rainfall (Rx1day - mm) of RSM between ENSO and non-ENSO. The large changes of Rx1day are detected over South China Sea, Tonkin and Thailand gulf and the western ICP. Rx1day tend to decrease about 5–10 mm over South China Sea and Tonkin gulf and increase about 5–10 mm over Thailand gulf and eastern Andaman Sea in both El Niño and La Niña. In Myanmar, rainfall tends to have a significant decrease in Rx1day with El Niño and a significant increase with La Niña.

3.4. Onset of summer rainfall season with ENSO and non- ENSO condition (reforecast 5-month)

The zonal wind is the most common monsoon index used in the world. The strengths of this indicator are the characteristics described of large-scale circulation, less impact of local factors and a very high correlation coefficient with the rain field. Before the date of monsoon onset, the zonal wind index is negative, it shows the stability of the easterly wind in the area.

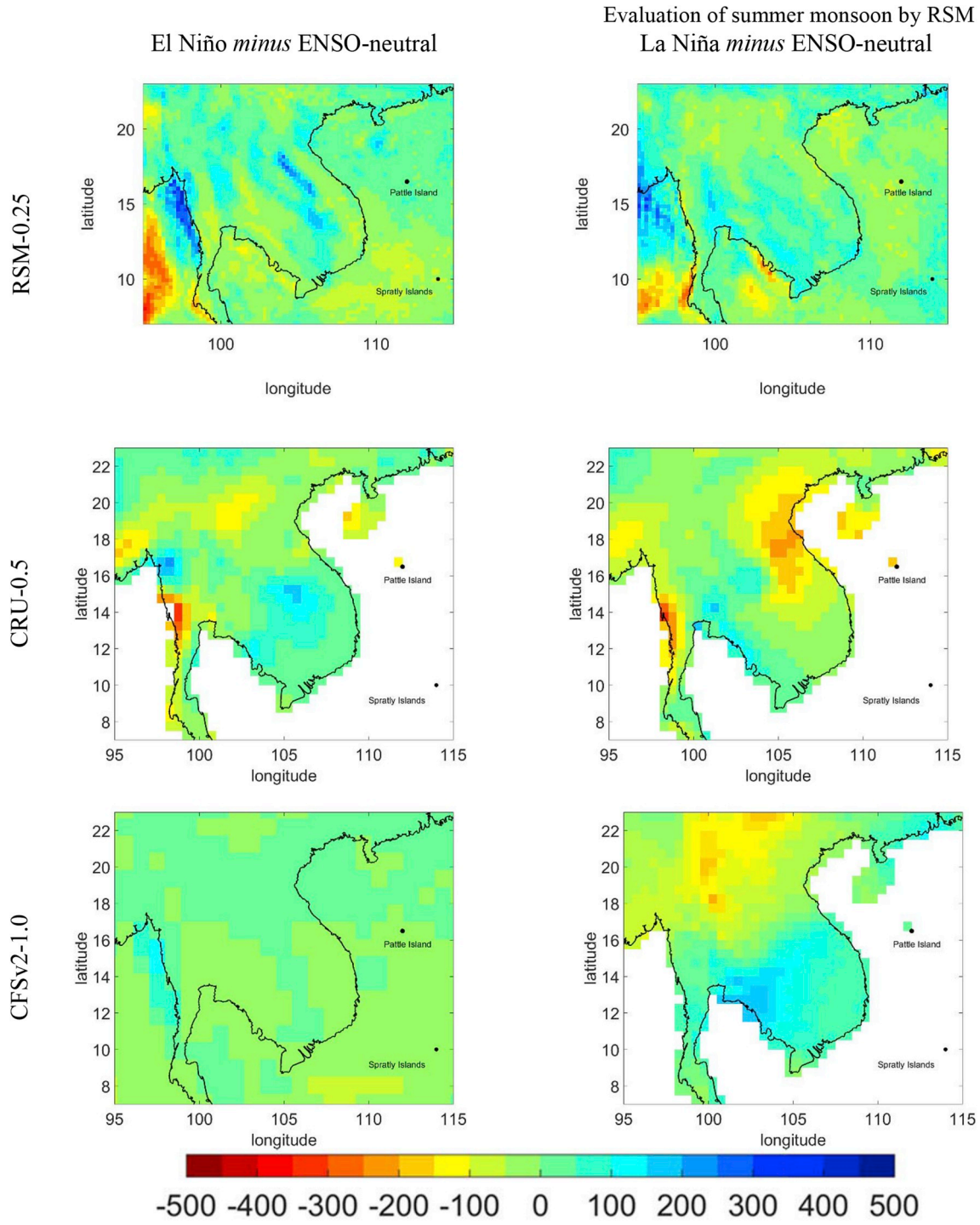

Fig. 7. Differences of total precipitation (mm) during summer (JJA) for different ENSO conditions of RSM-025 (above), of CRU-0.5 (middle) and CFSv2-1.0 (below).

Fig. 11 shows the onset date of summer monsoon. The onset of summer monsoon was defined by the change direction of western wind. RSM indicates that monsoon begins later with El Niño and earlier in case of non-ENSO by predictions and observation. It shows that RSM predicts good trend of monsoon development. However, it predicts the date of onset of the monsoon summer is later than CFS reforecast data about two weeks. Nguyen-Le et al. (2015) highlighted that summer monsoon tended to have early onset with La Niña condition due to the weakness of the western Pacific subtropical high. However, RSM result showed that the onset of summer monsoon with La Niña is similar with the one with non-ENSO condition and earlier than the one with El Niño.

Fig. 12 shows averaged domain-time daily rainfall from April to December based on 5 forecasts derived from RSM and CFSv2 with El Niño, La Niña and non-ENSO. Forecast-01 is from April to September; Forecast-02 is from May to October; Forecast-03 is from June to November; Forecast-04 is from July to December; Forecast-05 from August to the end of December. The result revealed the onset of summer rainfall over most of ICP region. The rainfall season often began about mid-May and ended the Late-November with the peak found in September and October. With El Niño, rainfall seemed to be higher than others at higher latitude, especially in September and October (about 15 mm/day) during monsoon season.

Outgoing Long-wave Radiation (OLR) data were observed at the top of the atmosphere. OLR are indicative of enhanced (suppressed)

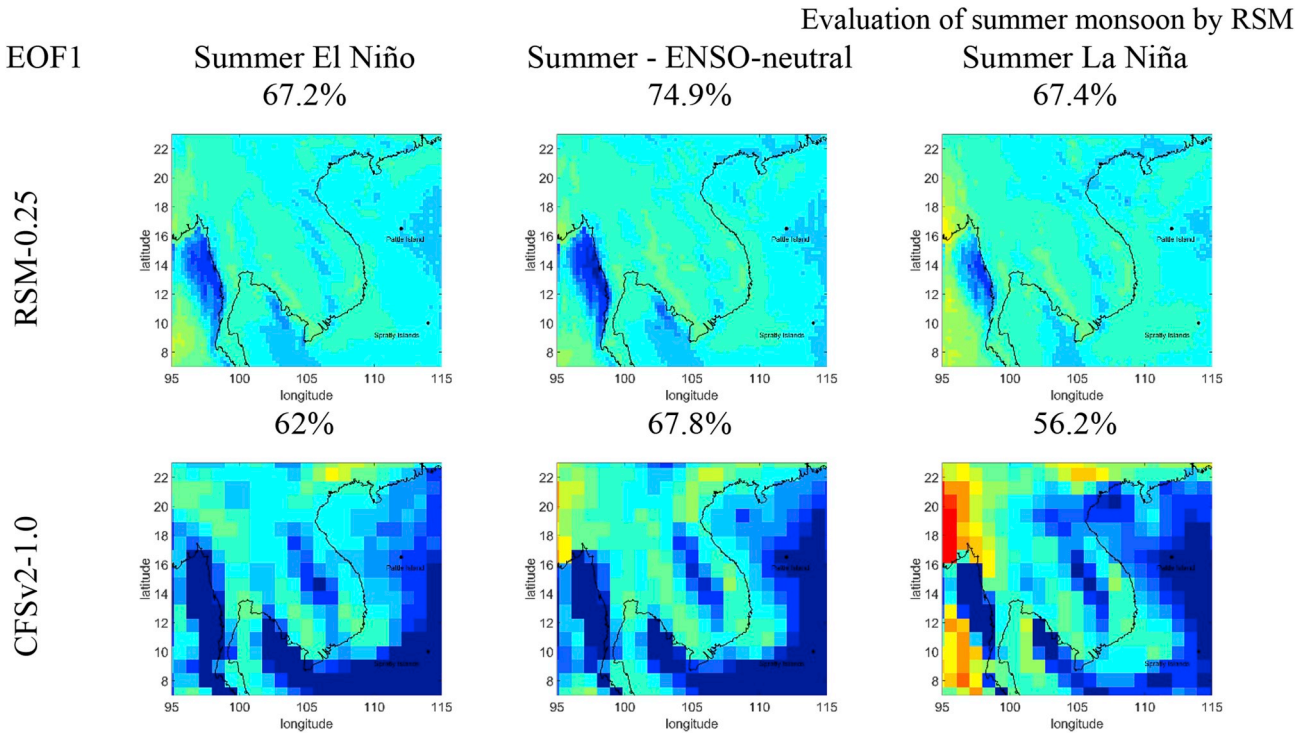

Fig. 8. Eigenvector patterns of leading EOF1 modes of daily rainfall over ICP in summers of El Niño/La Niña and ENSO-neutral conditions.

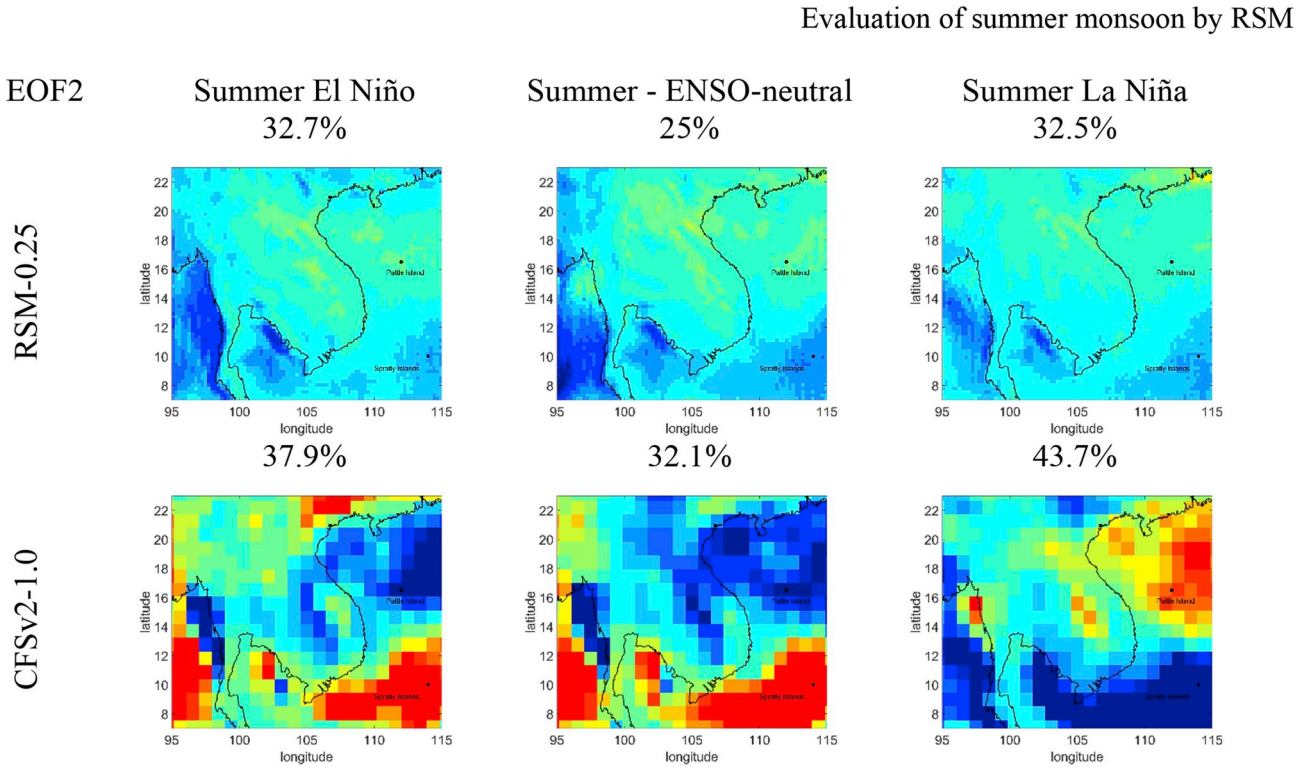

Fig. 9. Eigenvector patterns of leading EOF2 modes of daily rainfall over ICP in summers of El Niño/La Niña and ENSO-neutral conditions.

convection and hence more (less) cloud coverage typical of El Niño (La Niña) episodes. More (Less) convective activity implies higher (lower), colder (warmer) cloud tops, which emit much less (more) infrared radiation into space.

From the reforecast results with the five-month forecast period, there is a noticeable difference in the monthly averaged OLR during the case of El Niño, La Niña, and non-ENSO (Fig. 13). Specifically, in case of El Niño, the amount of OLR is quite large with common range from 200 to 300 W/m2 during April to December. Meanwhile, in the case of La Niña, the amount of OLR is lower than the case of El Niño, with prevalence from 220 to under 300 W/m2. Link with the rainfall forecast results; it shows that there is a discrepancy between the OLR value and the rainfall value. In particular, during the forecast period from May to October, the amount of OLR is reaching lows of around 200–260 W/m2.

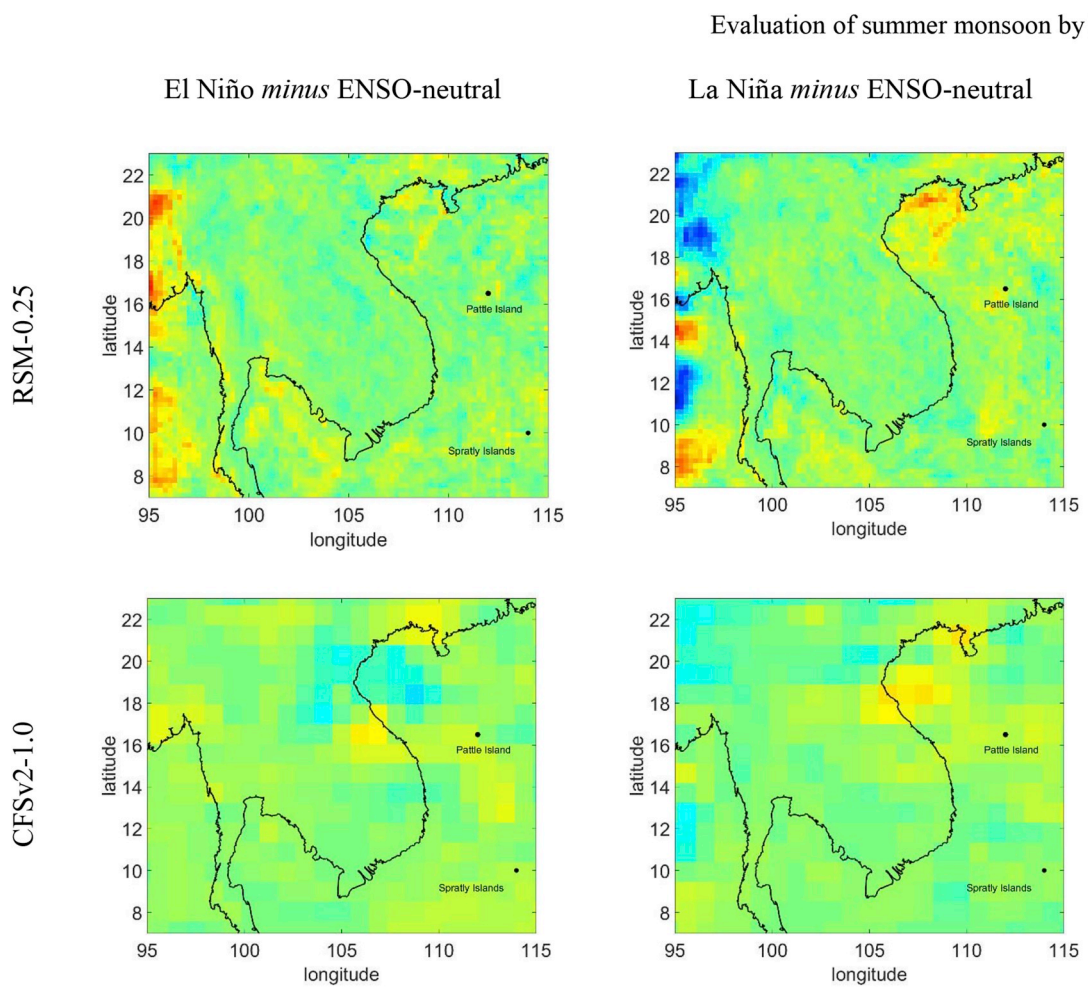

Fig. 10. Differences in averaged maximum rainfall in 1-day (Rx1day - mm) during summer (JJA) for different ENSO conditions of RSM-025 (above) and CFSv2-1.0 (below).

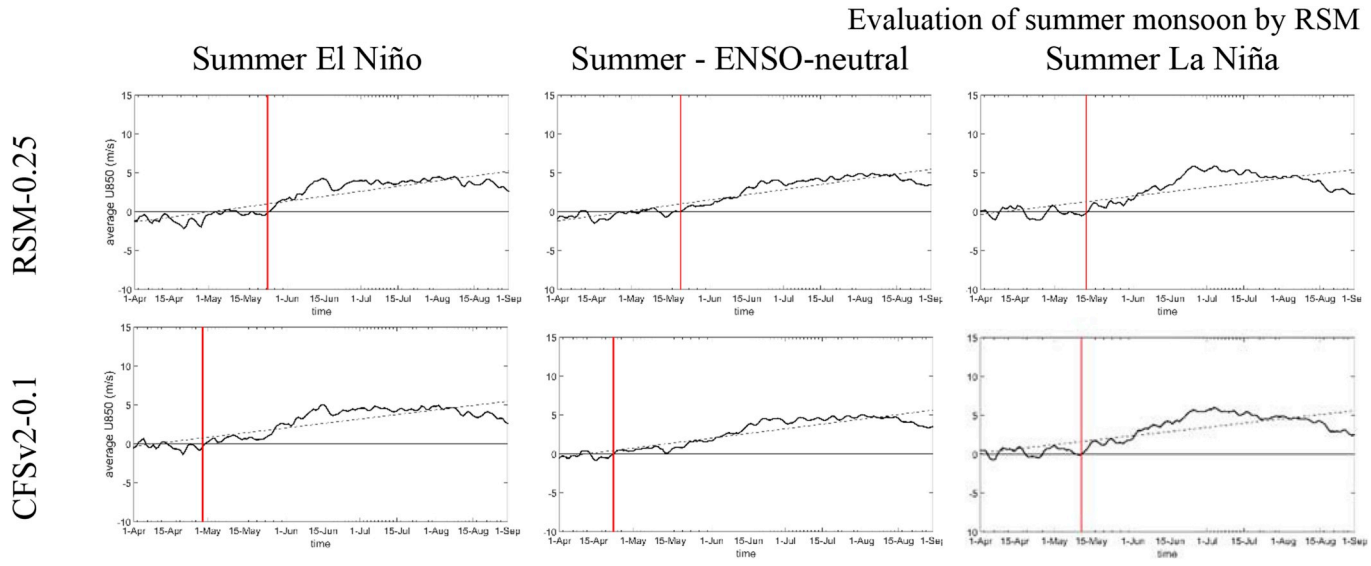

Fig. 11. Average U-wind (m/s) at 850 hPa level of RSM-0.25 and CFSv2-1.0 from April to September in summer of El Niño, Neutral and La Niña.

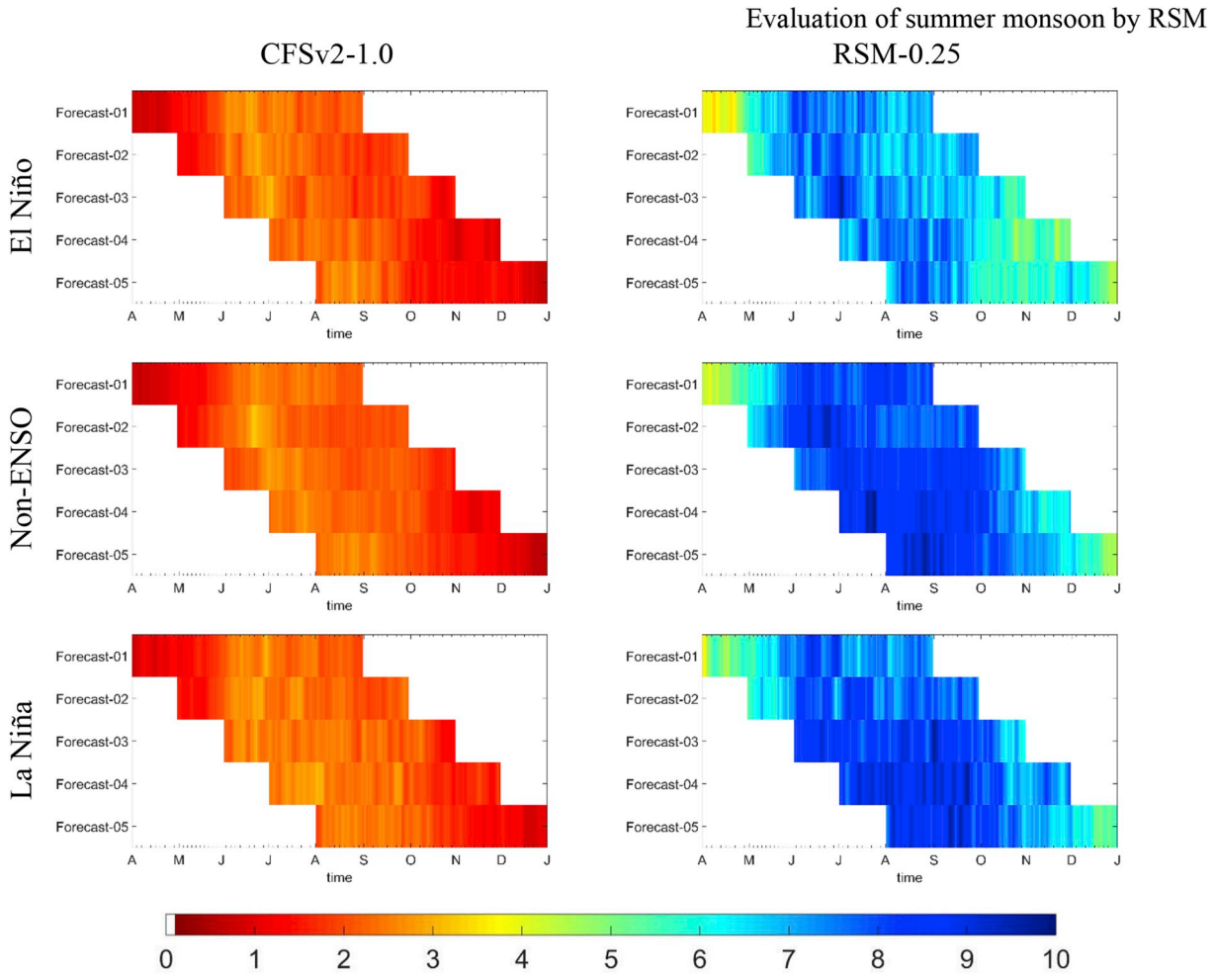

Fig. 12. Daily rainfall (mm) represented in averaged domain - time of CFSv2-1.0 (left) and RSM-0.25 (right) in summer of El Niño, Neutral-ENSO and La Niña. Forecast-01 from April to September; Forecast-02 from May to October; Forecast-03 from June to November; Forecast-04 from July to December; Forecast-05 from August to January.

Besides, the amount of precipitation is higher than other months (10–20 mm/day) (Fig. 12). In the forecast periods from April to May and November to December, the amount of OLR emitted are higher (around 250–300 W/m2), precipitation is in lower values, popular in the range of 0–5 mm/day. The results of the analysis show that the summer rain is rather late and occurs in the short period in the case of El Niño and occurs earlier in the case of La Niña.

4. Conclusion

Climate variables at 500, 700, 850 hPa and surface in summer of ENSO and non-ENSO derived from RSM were evaluated. The study shows that RSM can capture the signals of the impact of ENSO on climate system over the ICP region.

RSM forecasts Hgt consistent with the one of CFSR in pattern from north to south; however, the values are higher of about 10 m. For wind speed and direction, RSM seems to keep the wind fields similar to CFS-reforecast. The wind speed and direction are slower and inappropriate with those of CFSR. The distribution of the relative humidity in RSM and CFS-reforecast is comparable with CFSR; however, their values are higher than those of CFSR about 6% with El Niño and lower than 6% with La Niña.

The El Niño leads to increase of the surface temperature over seaside, but decrease over Thailand, Laos and Cambodia. Inversely, with the La Niña, the temperature decreases over the coastline when increasing over Cambodia and other areas. RSM reforecasts produce quite well the distribution of temperature in both conditions. For precipitation, RSM shows the reverse effects of ENSO condition over ICP. However, there is quite a difference in distribution when compared with CRU data.

The extremes maximum and minimum surface air temperature and maximum 1-day rainfall have been evaluated. El Niño and La Niña leads the maximum and minimum temperature change reversely over the IPC region. The maximum 1-day rainfall is also changed due to the ENSO condition, especially over sea and the western ICP.

This study demonstrated that summer rainfall was influenced by the disturbances in the southwest winds and from the south, which might be due to the MJO oscillation. In ENSO years, the changes of these systems lead to alter the summer rainfall. It is also evident that RSM predicts trends of monsoon development. With El Niño, summer monsoon begins later than the one with La Niña and non-ENSO. However, the model generally tends to predict monsoon activities earlier when compared to CFSR data for about two weeks.

Conflict of interest

The authors have read and understood the policy on declaration of interests and declare that there is no conflict of interest related to this article or legal bond or copy rights.

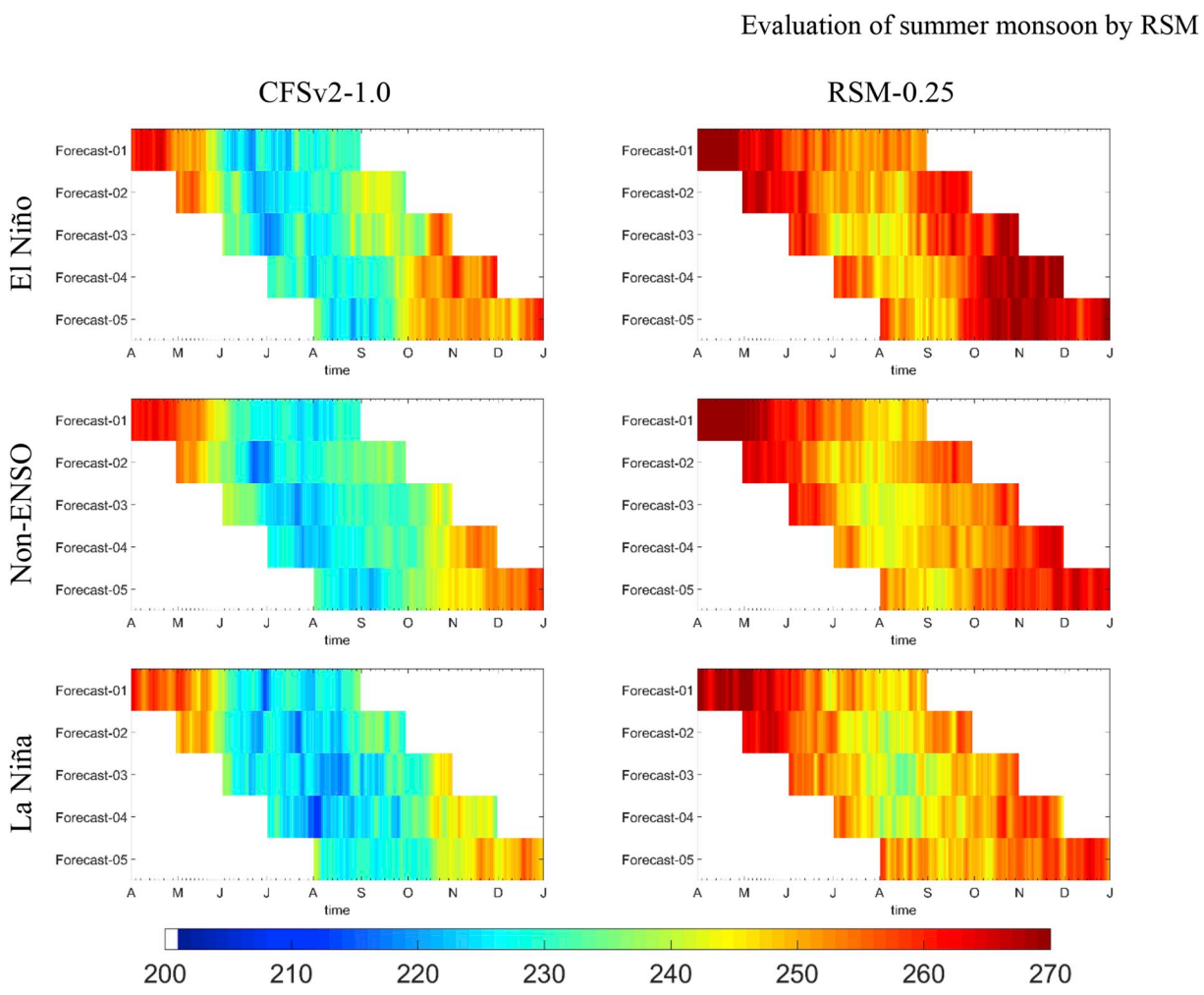

Fig. 13. Outgoing length radiation (W/m2) represented in averaged domain - time of CFSv2-1.0 (left) and RSM-0.25 (right) in summer of El Niño, Neutral-ENSO and La Niña. Forecast-01 from April to September; Forecast-02 from May to October; Forecast-03 from June to November; Forecast-04 from July to December; Forecast-05 from August to January.

Acknowledgments

This study was jointly supported by project development of seasonal climate forecasting system and by dynamic models for Vietnam - KC08.01/16–20. The authors wish to thank to our colleagues in the Center for Meteorology and Climatology (CMETC) for their very constructive comments, which significantly improved the paper.

Appendix A. Supplementary data

Supplementary data to this article can be found online at https://doi.org/10.1016/j.wace.2019.100195.

References

Chou, M.-D., Suarez, M.J., 1999. A Solar Radiation Parameterization for Atmospheric Studies 15 National Aeronautics and Space Administration, Goddard Space Flight Center, Laboratory for Atmospheres, Climate and Radiation Branch: Laboratory for Hydrospheric Processes, NASA Seasonal-to-Interannual Prediction Project.

Ek, M.B., Mitchell, K.E., Lin, Y., Rogers, E., Grunmann, P., Koren, V., Gayno, G., Tarpley, J.D., 2003. Implementation of Noah land surface model advances in the National Centers for Environmental Prediction operational mesoscale Eta model. J. Geophys. Res.: Atmosphere 108 (D22).

Grell, G.A., 1993. Prognostic evaluation of assumptions used by cumulus parameterizations. Mon. Weather Rev. 121 (3), 764–787.

Han, J., Roads, J.O., 2004. US climate sensitivity simulated with the NCEP regional spectral model. Climatic Change 62 (1–3), 115–154.

Harris, I.P.D.J., Jones, P.D., Osborn, T.J., Lister, D.H., 2014. Updated high-resolution grids of monthly climatic observations–the CRU TS3. 10 Dataset'. Int. J. Climatol. 34 (3), 623–642.

Ju, J., Slingo, J., 1995. The Asian summer monsoon and ENSO. Q. J. R. Meteorol. Soc. 121 (525), 1133–1168.

Juang, H.-M.H., Kanamitsu, M., 1994. The NMC nested regional spectral model. Mon. Weather Rev. 122 (1), 3–26.

Juang, H.-M.H., 2000. The NCEP mesoscale spectral model: A revised version of the nonhydrostatic regional spectral model. Mon. Weather Rev. 128 (7), 2329–2362.

Juang, H.-M.H., Hong, S.-Y., 2001. Sensitivity of the NCEP regional spectral model to domain size and nesting strategy. Mon. Weather Rev. 129 (12), 2904–2922.

Matsumoto, J., 1997. Seasonal transition of summer rainy season over Indochina and adjacent monsoon region. Adv. Atmos. Sci. 14 (2), 231–245.

Mlawer, E.J., Taubman, S.J., Brown, P.D., Iacono, M.J., Clough, S.A., 1997. Radiative transfer for inhomogeneous atmospheres: RRTM, a validated correlated-k model for the longwave. J. Geophys. Res.: Atmosphere 102 (D14), 16663–16682.

Nguyen, D.N., 2017. 'Impact of ENSO on Extreme Temperature in Viet Nam', Vietnam Journal of Science and Technology.

Nguyen-Le, D., Matsumoto, J., Ngo-Duc, T., 2014. Climatological onset date of summer monsoon in Vietnam. Int. J. Climatol 34 (11), 3237–3250.

Nguyen-Le, D., Matsumoto, J., Ngo-Duc, T., 2015. Onset of the rainy seasons in the eastern Indochina Peninsula'. J. Clim. 28 (14), 5645–5666.

Saha, S., Moorthi, S., Pan, H.L., Wu, X., Wang, J., Nadiga, S., Tripp, P., Kistler, R., Woollen, J., Behringer, D., 2010. & others. In: NCEP Climate Forecast System Reanalysis (CFSR) 6-hourly Products, January 1979 to December 2010. Research Data Archive at the National Center for Atmospheric Research, Computational and Information Systems Laboratory, Boulder, CO.

Saha, S., Moorthi, S., Wu, X., Wang, J., Nadiga, S., Tripp, P., Behringer, D., Hou, Y.-T., Chuang, H.-y., Iredell, M., others, 2014. The NCEP climate forecast system version 2'. J. Clim. 27 (6), 2185–2208.

Troen, I.B., Mahrt, L., 1986. A simple model of the atmospheric boundary layer; sensitivity to surface evaporation. Boundary-Layer Meteorol. 37 (1–2), 129–148.

Wang, B., 2002. Rainy season of the Asian–Pacific summer monsoon. J. Clim. 15 (4), 386–398.

Webster, P.J., Yang, S., 1992. Monsoon and ENSO: selectively interactive systems. Q. J. R. Meteorol. Soc. 118 (507), 877–926.
Zhang, Y., Li, T., Wang, B., Wu, G., 2002. Onset of the summer monsoon over the Indochina Peninsula: Climatology and interannual variations. J. Clim. 15 (22), 3206–3221.
Zhang, Y., Chen, Y.-L., Hong, S.-Y., Juang, H.-M.H., Kodama, K., 2005. Validation of the coupled NCEP mesoscale spectral model and an advanced land surface model over the Hawaiian Islands. Part I: summer trade wind conditions and a heavy rainfall event. Weather Forecast. 20 (6), 847–872.
Zhou, W., Chan, J.C.L., 2007. ENSO and the South China Sea summer monsoon onset. Int. J. Climatol. 27 (2), 157–167.